Topological characterisation of a chaotic attractor with an additional branch generated from economic data

Alexandre Meneceur, Vincent Lignon, Martin Rosalie

Nonlinear Science 5 (2025) 100070

Contents lists available at ScienceDirect

Nonlinear Science

journal homepage: www.elsevier.com/locate/nls

Research paper

Topological characterisation of a chaotic attractor with an additional branch generated from economic data

Alexandre Meneceur [a,b], Vincent Lignon [b], Martin Rosalie [a,*]

[a] Laboratoire Génome et Développement des Plantess (LGDP), UMR 5096, Université de Perpignan Via Domitia, CNRS, Avenue P. Alduy, Perpignan, 66860, France

[b] Centre de Droit Économique et du Développement Yves Serra, Université de Perpignan Via Domitia, Avenue P. Alduy, Perpignan, 66860, France

ARTICLE INFO

Dataset link: https://github.com/ameneceur/economic-attractor-topology

Keywords:
Global modelling
GPoM
Chaotic dynamics
Topological characterisation
Economic data
Phillips curve
Unemployment
Inflation

ABSTRACT

There are insights of chaotic properties in economic systems and data. To prove the existence of chaotic dynamics, the establishment of a deterministic model is mandatory. A global modelling tool (GPoM) is used to search for mathematical models of equations from economic data: unemployment, inflation and nominal exchange rate over 30 years. A system of three differential equations is selected as a model, whose solution is a chaotic attractor in $\mathbb{R}^3$. The model extracted from the data is not able to fit them, but it provides equations linking those multiple economic variables. The topological characterisation of the chaotic attractor solution exhibits an additional branch in its first return map to the Poincaré section. Consequences of this particular structure are analysed and interpreted economically.

1. Introduction

Economic dynamics are made of complex systems with multiple interactions that often defy precise forecasting. This difficulty is further compounded by the nonlinear nature of the relation between economic aggregates and their propensity to oscillate between periods of stability and instability [1]. As a consequence, the investigation of chaotic dynamics within economic systems has emerged as a significant area of research [2,3]: this exploration is motivated by the limitations of linear models in capturing the complexities and nonlinearities inherent to economic phenomena. There exist tools that compute values giving insight on the fact that chaos could appear in economic systems [4,5]. Since chaos is by nature deterministic, any claim of chaotic behaviour must first demonstrate the underlying determinism [6].

The methodologies employed in economics can be broadly categorised into two distinct approaches. The foremost and significantly most prevalent method *(the structural approach)* involves the construction of theoretical economic models that, through specific parametrisations or structural designs, exhibit chaotic behaviour. It often begins with established economic frameworks, such as general equilibrium models and introduces nonlinear elements or mechanisms that can generate complex dynamics [7].

The second one, which is more investigative and less developed *(the empirical approach)*, focuses on the empirical analysis of economic data to detect the presence and characteristics of chaotic dynamics: it seeks to identify chaotic patterns directly from observed economic data, such as stock prices, exchange rates, or macroeconomic indicators. Based on a single time series, Elena Olmedo [4] has for instance underlined that unemployment in Spain behave in a chaotic way.

* Corresponding author.
E-mail addresses: vincent.lignon@univ-perp.fr (V. Lignon), martin.rosalie@univ-perp.fr (M. Rosalie).

https://doi.org/10.1016/j.nls.2025.100070
Received 17 July 2025; Received in revised form 9 October 2025; Accepted 10 October 2025
Available online 14 October 2025

The purpose of the paper is to provide a topological characterisation and interpretation of a chaotic attractor generated from economic data. We go further in the empirical approach of chaos in economics using a set of three times series data taken from the specific context of French economy.

Let us emphasise at the outset that our goal is not to build an economic model, nor to predict or fit the data, but rather to extract structure and dynamical properties from time series to have insight on the mechanisms relating multiples economic variables. While traditional metric methods (Lyapunov exponents, correlation dimension, BDS tests) struggle to detect chaotic signatures in economic data due to their sensitivity to noise, non-stationarity, and limited sample sizes [8], a topological analysis of attractors provides a robust alternative [9]. By focusing on topological characterisation, we aim to complement existing empirical approaches and provide interpretative insights into the complex interactions relating multiples economic variables.

The data series selected correspond to a classic topic in economics: the Phillips curve, which traditionally links inflation and unemployment [10]. This framework provides a rich ground for exploring complex dynamics. The Phillips curve posits an inverse relationship between inflation and unemployment, suggesting a trade-off that policymakers can exploit. However, the stability and predictability of this relationship have been questioned over time, with empirical evidence suggesting that the Phillips curve can shift or even disappear under certain conditions [11,12]. Building on recent advancements in the field, we incorporate a third dimension – the nominal exchange rates – into our analysis. This addition is motivated by the work of François Geerolf [13], who argues that the conventional interpretation of the Phillips curve may overlook critical complexities in modern economies. Specifically, he highlights the pivotal role of exchange rates in shaping the dynamic interplay between unemployment and inflation.

In this framework, we propose to use tools such as GPoM [14] to generate systems of differential equations from three economic time series (price inflation, unemployment and the nominal exchange rate). Since these tools generate systems of differential equations involving polynomial and nonlinear terms, solving these systems may yield chaotic attractors as solutions. Currently, several tools can help to describe, characterise and classify these chaotic dynamics [15–17]. The solution of the obtained system exhibits a particular structure with a unimodal first return map to the Poincaré section with an additional branch. Such a particular structure can be interpreted in multiple ways as a prolongation in the template [18–20] or as an extra branch [21,22]. Theoretical results presented hereinafter using the Rössler system [23] will clarify the role of such an additional branch. Finally, the topological analysis of the chaotic attractor solution of a model will provide some details on the dynamics and its implication on the economical interpretations.

2. Topological characterisation method

Further to this recent review [17], chaos is defined as follows: "A more practical definition could be that a solution S to a dynamical system $f : \mathbb{R}^d \to \mathbb{R}^d$ is said to be chaotic if f is deterministic, S is bounded, and S is sensitive to initial conditions". Consequently, the deterministic aspect of models is fundamental to obtain chaos and, the differential equations systems obtained from global modelling techniques ensure this property. Literature on *chaotic dynamics* and *nonlinear dynamics* has been developed at the end of the century while the main concepts of this theory come from the early nineties (see Fig. 1 of [24]).

For a detailed introduction to the topological approach to chaotic dynamics, see the book "*The Topology of Chaos: Alice in Stretch and Squeezeland*" by Gilmore and Lefranc [25]. Fig. 1 represents the steps of the topological characterisation of a chaotic attractor solution to a standard system in the domain [26]. The Rössler system [23]:

$$\begin{cases} \dot{x} = -y - z \\ \dot{y} = x + ay \\ \dot{z} = b + z(x - c) \end{cases} \tag{1}$$

has the attractor $\mathcal{R}$ (Fig. 1a) solution for parameters $a = 0.398$, $b = 2$ and $c = 4$.

The main tools developed for analysing attractors solution of dissipative systems are the Lyapunov Exponents (quantification of the rate of separation for infinitesimally closed trajectories), and the Poincaré section (Fig. 1b) whose purpose is to transform a continuous problem to a discrete representation of trajectories and their link after a topological period. For the Rössler system, the Poincaré section is defined as follows:

$$\mathcal{P} = \left\{(y_n, -z_n) \in \mathbb{R}^2 \mid -x_n = -x_-,\ -\dot{x}_n < 0\right\} \tag{2}$$

where x_- is a x-value of the central fixed point of the system. From this Poincaré section, a variable ρ_n is defined to represent the distance from the inside of the attractor to the outside:

$$\rho_n = 1 - (y_n + 4.98)/(-2.15 + 4.98) \tag{3}$$

This variable is used to build the *first return map* that is the signature of the chaotic dynamics (Fig. 1c). Unstable Periodic Orbits (UPOs) are considered as the skeleton of a chaotic attractor because of their unstable property (Fig. 1d) [26]. Consider that a differential equations system is numerically solved (using the four-order Runge–Kutta algorithm, RK4), the solution is a trajectory in a phase space. Thus, at a moment, this numerical solution of a differential equations system will "follow" one UPO for a while before diverging and visiting another UPO. This process maintains the trajectory into the attractor; the latter being the solution of the differential equations system that cannot be described analytically. The "periodic" in periodic orbits refers to the state space and not to the time space (topological period). Periodic orbits are time invariant while the system evolves in a chaotic state (from initial condition, the solution evolves and successively visits the unstable periodic orbits). From a chaotic time series that is the numerical

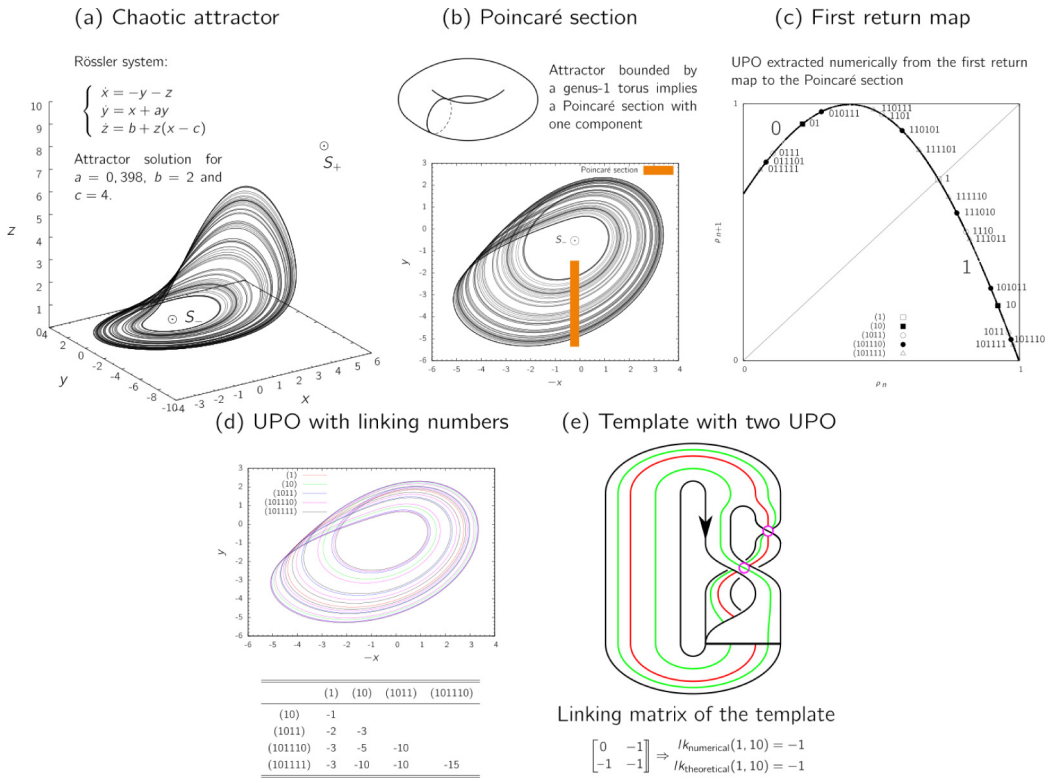

	(1)	(10)	(1011)	(101110)
(10)	-1			
(1011)	-2	-3		
(101110)	-3	-5	-10	
(101111)	-3	-10	-10	-15

$$\begin{bmatrix} 0 & -1 \\ -1 & -1 \end{bmatrix} \Rightarrow \begin{matrix} lk_{\text{numerical}}(1,10) = -1 \\ lk_{\text{theoretical}}(1,10) = -1 \end{matrix}$$

Fig. 1. Topological characterisation of a chaotic attractor (adapted from Fig. 1 of [27]). (a) $\mathcal{R}$ is the chaotic attractor solution of the Rössler system (1). (b) Bounding torus of the attractor indicating the required number of components to create the appropriate Poincaré section. The Poincaré section (2) is represented in the phase space with a flow evolving clockwise. (c) First return map with periodic points indicating the position of the Unstable Periodic Orbits (UPOs). (d) Numerical representation of the UPOs in the phase space and table containing numerical linking numbers between UPOs. (e) Template describing the topological properties of the attractor. Linking matrix detailing torsions and permutations for each branch in the template with the validation when theoretical linking numbers (computed from the linking matrix and the joining chart) between orbits correspond to numerical linking numbers (d).

solution of a differential equations system, UPOs can be extracted from the first return map, and this acquisition is a preliminary step of the *topological characterisation* [28]. For dissipative systems, the purpose of this method is to obtain the structure of the chaotic attractor from a topological invariant (the linking number Fig. 1d) computed between every couple of UPOs (the reader is referred to [25] for details). The template was originally introduced as "knot-holder" by Birman and Williams [29] that permits to resume the topological properties of the topological invariants extracted from the attractor using the linking number (Fig. 1e). The template is a formal description of the branched manifold detailing the topological properties of a chaotic attractor. The linking numbers between each pair of orbits are computed numerically (Fig. 1d) and theoretically using the algebraic description of the template by the linking matrix R

$$R = \begin{bmatrix} 0 & -1 \\ -1 & -1 \end{bmatrix}. \tag{4}$$

and linking graphs. The linking matrix indicates the torsions and permutations between orbits, but additional crossings could happen in the joining chart. Templates are constructed under the Tufillaro's convention [30] where, before the stretching and squeezing mechanism of the template, the left to right order corresponds to the bottom to top order, inducing only positive crossing in linking charts as illustrated by transparency in Fig. 1e. The template is validated if both, theoretical and numerical linking numbers, are equals for corresponding couple of UPO (Fig. 1e). A template is described with a linking matrix detailing the number of branches with their torsions and how they permute before joining. The template of the Rössler attractor is thus defined by the linking matrix R (4). This formalism underlines the chaotic properties of the attractor with a splitting chart that separate the flow in branches (sensitivity to initial conditions with the stretching and folding part of the mechanism) and a joining chart where trajectories are regrouped before going for another round (bounded solution). Templates of various chaotic attractors solution to a Rössler system have been established using this framework [31].

Table 1
Stationarity tests on raw and smoothed data (unemployment rate: x, inflation rate: y and nominal effective exchange rate: z).

Test (criterion for stationarity)	Raw data $p-$values (x, y, z)	Smoothed data $p-$values (x, y, z)
KPSS ($p-$value > 0.05)	**0.0718**, **0.1**, **0.0938**	0.01, 0.01, 0.01
PP ($p-$value < 0.05)	0.5658, 0.0828, 0.2764	0.8324, 0.6182, 0.7226
ADF ($p-$value < 0.05)	0.543, 0.2919, 0.0994	0.0946, **0.01**, 0.1448

3. Modelling economic data and chaotic solution

3.1. Global modelling

The global modelling technique initiated in the early 1990s [32–34] aims to extract differential equations systems directly from observational time series. Originally, it was mostly applied to single time series and to either theoretical [33,35] or experimental cases [36]. Applications to multivariate time series from real environmental conditions is recent [37]. Few tools have been developed for this purpose. The Generalised Global Polynomial Modelling (GPoM) package [14,38] developed at Cesbio by S. Mangiarotti is one of them. Another popular technique, the Sparse Identification of Nonlinear Dynamics (SINDy) tool [39], was proven to be quicker, but its ability to obtain non trivial approximations of environmental dynamics remains uncertain. GPoM is relatively slower when applied to already known systems because its algorithm systematically checks the numerical integrability of the equations which is time-consuming. This test of integrability becomes mandatory when the original equations are unknown, and then, GPoM cannot be considered as slower anymore. This limitation for numerical integration has been addressed via parallelisation and will be made available in the new versions of the package (S. Mangiarotti, personal communication, June 5 2025). From this point of view, the GPoM platform has proven to be particularly interesting. It was successfully applied to numerous realms, which makes it the best candidate for the present project. Since the early 2010s, it has been successfully applied to agronomy of cereal crops cycles [40], geohydrology of karstic systems [41], eco-epidemiology of plague [37], epidemiology of Ebola and COVID-19 [42], eco-hydrology of earthworms activity [43], and seasonal cycles of CO_2 in caves [44].

GPoM can be used with different objectives: (1) for dynamical characterisation (chaos detection and topological classification); (2) for coupling detection (in particular under highly nonlinear conditions), and (3) for retro-modelling (that is, to obtain interpretable equations). Note that for this latter objective, in a single case, a complete interpretation of the differential equations systems obtained from observational time series could be proposed, [37] which reveals the potential of the approach. The GPoM package is an open-source package developed in R language and made available on the Comprehensive R Archive Network (CRAN) [45].

3.2. Economic data, pre-treatment and origin

A set of three-monthly time series is considered; each associated to a macroeconomic variable in the French setting. Those variables have been chosen accordingly to the recent debates on the Phillips curve mentioned above [13]. The time series on unemployment and inflation come from the INSEE (National Institute of Statistics and Economic Studies) [46] database, whereas the time series on exchange rate comes from the BIS (Bank for International Settlements) [47] database over 30 years. Fig. 2 represents the time series of the three variables:

- Unemployment rate (the share of the labour force that is unemployed and actively seeking employment)
- Inflation rate (the percentage increase or decrease in the price level of goods and services in the economy over a year)
- Nominal effective exchange rate (a measure of the value of a country's currency relative to a weighted basket of foreign currencies)

A noteworthy point is that stationarity tests (KPSS, PP, ADF) [48–50] have been run using `tseries` library [51] on the data (Table 1), suggesting that the studied series might not be stationary, even though KPSS tests on raw data suggest stationarity.

According to the GPoM documentation, it is often necessary to subsample the time series, before resampling them using spline interpolation, as giving a polynomial form to the curves may help the algorithm succeed in finding a nonlinear dynamic. The values of the time series are also normalised in $[0, 1]$ in a homogenisation matter (see second column of Fig. 2). The GPoM algorithm is then applied to the set of time series, with different parameters to ensure that most combinations of polynomial terms are covered by the algorithm. A set of prestructured models is then generated and are tested in terms of numerical integrability (diverging models are rejected). The remaining models are then selected by default, based on their performances to reproduce the original phase portrait. Two closely related models emerged (with a solution that neither converges to a point nor diverges after long time of integration), either with small variations in parameter values and/or with an additional term in one of the equations. We selected the model with fewer equation terms whose solution is not periodic oscillations.

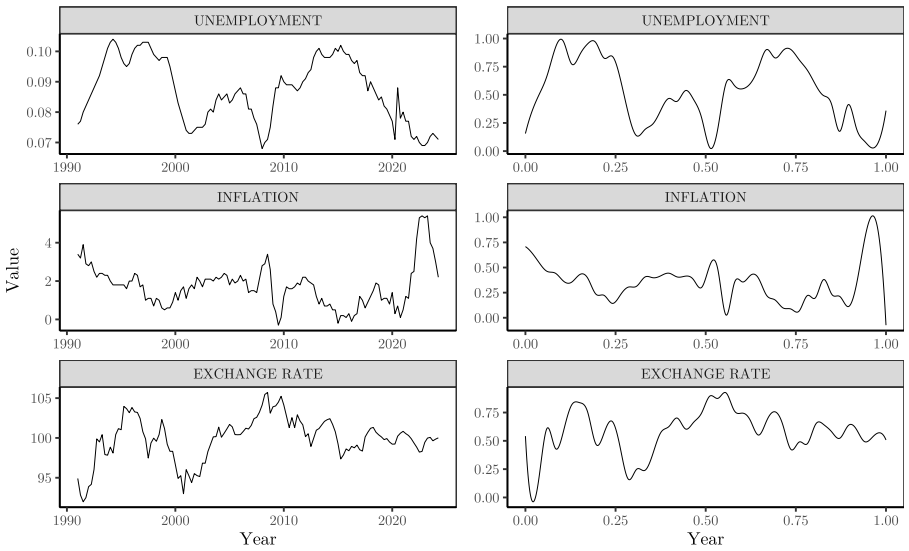

Fig. 2. The original time series and the normalised and preprocessed time series (second column) used to perform global modelling with GPoM.

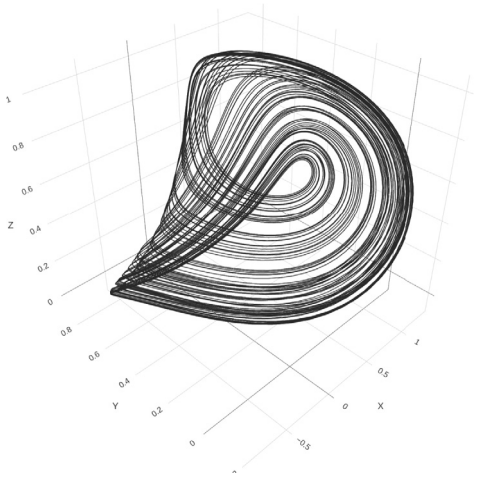

Fig. 3. Attractor $\mathcal{E}$ solution of the model (5).

3.3. Model

For the reminder of this article, the following notation is used:

- Unemployment rate (x)
- Inflation rate (y)
- Nominal effective exchange rate (z)

and the selected model generated by GPoM is defined as follows:

$$\begin{cases} \dot{x} = -15.2193492215949 + 12.6246703650997\ z + 12.2891205846936\ z^2 + 38.2077775976987\ y - 51.327806215602\ yz \\ \dot{y} = 11.3194672143246\ z - 11.1810798067421\ z^2 - 4.59572630441015\ x \\ \dot{z} = -5.1609358283762\ xz + 10.5277054934486\ xy \end{cases} \tag{5}$$

First, it indicates that the data could be connected using these relations. The solution of this system is a chaotic attractor $\mathcal{E}$ (Fig. 3). As our purpose is not to fit the trajectories but rather to examine whether a relationship exists between these variables and what its properties are, this mathematical model is a way to reveal the complex underlying dynamics contained in the data. As deriving a deterministic model from random-like data is deemed highly unlikely [52], the fact that such a model can be obtained provides evidence for an underlying structure that merits analysis.

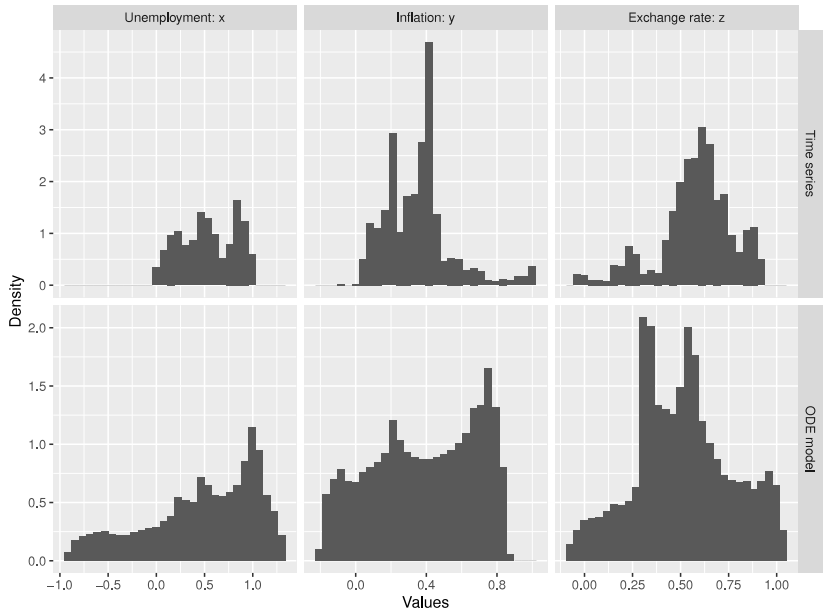

Fig. 4. Density histograms of values (x, y, z) of both time series and solution of the model (5).

3.3.1. Relating model outputs to observed data

Running a data/model consistency analysis with very short time series is inherently challenging. In our case, the model was run over a much longer timescale than the empirical observations, making its output distribution a faithful reflection of its equations. Consequently, the empirical and simulated distributions are not expected to be identical.

Density histograms (Fig. 4) display the distribution of model outputs and observed time series by showing the relative frequency of observations across intervals, normalised to represent probability density. Because the empirical series is much shorter than the simulated one, the empirical distribution can reasonably be expected to lie within the range of the model distribution, which is largely the case. Given this limitation, the distributions appear broadly compatible: the empirical values are contained within the model range, except for a small discrepancy for the largest values of observed inflation (data reaches 0.9 whereas model does not exceed 0.85). However, this deviation concerns only a very thin tail of the distribution.

The model reproduces the three peaks observed in the unemployment distribution. However, the absence of a clear tail in the data could reflect the short length of the empirical time series or a genuine discrepancy. Similarly, the three peaks in the exchange rate distribution are recovered, although their exact positions differ slightly between the model ($\sim 0.31, \sim 0.54, \sim 0.96$) and the data ($\sim 0.27, \sim 0.61, \sim 0.88$). In contrast, the comparison for inflation is less satisfactory: only one peak (at 0.2) coincides, while the most prominent empirical peak (at 0.4) is not reproduced. Once again, these divergences may arise both from the limited length of the observed series and from the fact that the model constitutes a low-dimensional approximation of the complex dynamics observed.

These distribution comparisons allow us to establish connections between the model (5) and the available data. It is important to remember that our objective is not to fit the data or predict the evolution of the time series, but rather to analyse the dynamics emerging from the system of differential equations that link these economic variables.

3.3.2. Interpretation

It should be noted that the model generated by GPoM highlights relationships that are partly consistent with the theoretical framework proposed by the Phillips Curve and its developments [13]. It reflects, for instance, the intuition that the unemployment rate has a negative impact on inflation, which is consistent with the idea that an improvement in the situation on the labour market maintains upward pressure on prices (through higher household consumption and greater bargaining power of employees). Besides, the nominal exchange rate has a positive (and cumulative) impact on the unemployment rate. One possible interpretation is that an appreciation of the national currency (i.e. the exchange rate) can lead to a loss of competitiveness for the country (the price of exported products being more expensive for non-resident economic agents). In this context, when the currency appreciates, export-oriented industries may experience a drop-in activity and lay off part of their workforce.

Within our exploratory framework, it is important to remember that some interactions highlighted by the model are not addressed by theoretical frameworks in economics, which predominantly focus on the implications of anticipated inflation and equilibrium conditions. By contrast, our empirical methodology examines the subject through a different lens, suggesting that the nominal exchange rate could play a role in the cross-relation between inflation and unemployment (insofar as the exchange rate depends on the central bank's monetary policy reactions). For instance, the evolution of the unemployment rate depends on the level of inflation, but the sign of this effect is conditional on the level of the nominal exchange rate. In other words, there could be one or

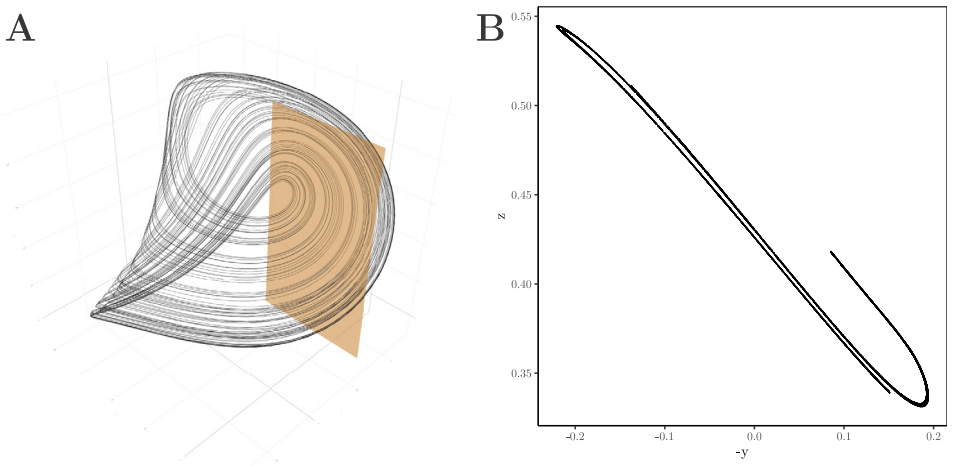

Fig. 5. A. Three-dimensional representation of the chaotic attractor solution $\mathcal{E}$ and the Poincaré section $\mathcal{P}$. B. Computed points of $\mathcal{P}$.

more nominal exchange rate thresholds that could have a strong impact on the combined dynamics of unemployment and inflation. These cross-relationships involving the exchange rate (and therefore central bank intervention) can lead to very different dynamics that could be taken into account in theoretical modelling (e.g., an example of modelling [53]). As the model outputted by GPoM is not an economic model, it can only be considered as a rough approximation of the original economic dynamic, and it does not allow for a full interpretation of all the terms in the system's equation. However, since the system was derived from the data, it contains information about their relationships, which we analyse below.

4. First return map with additional branches

4.1. First steps of the topological characterisation

The topological analysis is performed as previously defined (Section 2). The flow evolves clockwise in the phase plane $(x - y)$. The Poincaré section is the hyperplane $\mathcal{P}$ (represented in Fig. 5.A) defined as follows:

$$\mathcal{P} = \left\{(y(t), z(t)) \in \mathbb{R}^2 \ | x(t) = x_-,\ y(t) < y_-,\ t > 0\right\}$$

Fig. 5B shows the Poincaré section with the orientation of the y–axis from the inside to the outside of $\mathcal{E}$. This Poincaré section exhibits a particular structure where there are several layers that corresponds to chaotic dynamics signature where the flow is stretched, folded and squeezed. There is no possibility to position a Poincaré section on $\mathcal{E}$ without having such a structure with multiple layers. The first return maps of attractors solution to system generated from non-stationary data show additional structures [54]; this is observed in Fig. 5B. However, strong non-stationarity leads to the appearance of numerous additional structures that are concentrated and overlap in the first return maps. In our case, the additional structure is a simple additional branch without overlapping. This corroborates the statistical analysis where data used for modelling are weakly non-stationary. To precisely understand the implication of such a constraint on topological characterisation, we first address this problem with the well known Rössler system [23].

4.2. The case of the Rössler attractor

Additional branches in first return maps can be observed, but their impact on the topological characterisation is not clear (see [18–20] where extra-branches are not considered and reciprocally [21,22] where they are considered). These extra-branches must be distinguished from foliated structure exhibited by Lorenz system [55] and Chen system [56] where the foliations are the result of a tearing mechanism [57]. As a first glimpse on the system (5) solution, it appears that several folding might occur (Fig. 3) without tearing mechanism. The purpose of this subsection is to clarify the meaning of an additional branch in first return map where only stretching and folding mechanisms occurs (see template Fig. 1e). First return maps depend on the Poincaré section's position used to perform the topological characterisation of an attractor (see [58] for four distinct first return maps for only one chaotic attractor). A first return map is obtained with an extra branch (Fig. 7A) using the Rössler system (1) with the following Poincaré section:

$$\mathcal{Q} = \left\{(y_n, -z_n) \in \mathbb{R}^2 \ | -x_n = -1,\ -\dot{x}_n > 0\right\} \tag{6}$$

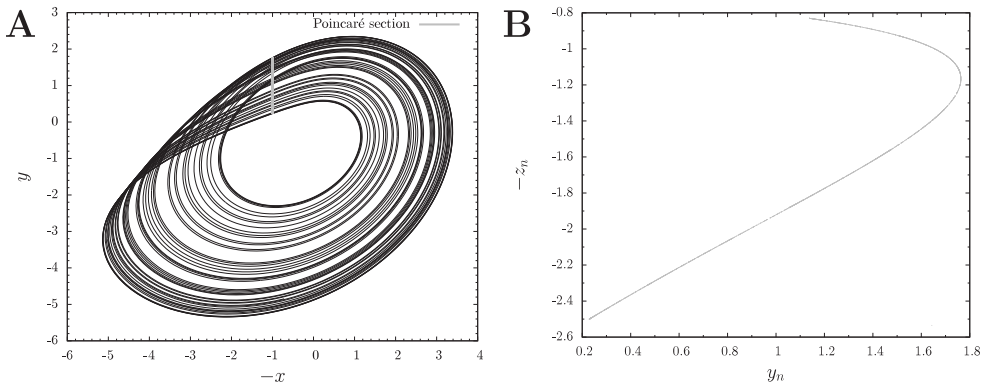

Fig. 6. Poincaré section positioned inside the stretching and folding mechanisms. A. Space phase $(-x, y)$ with flow evolving clockwise with the Poincaré section $\mathcal{Q}$ (6) place in the stretching and folding mechanism. B. Poincaré section $\mathcal{Q}$ (6) in $(y_n, -z_n)$. The only use of y_n to build a variable γ_n remove the bijection between the section and the Poincaré section.

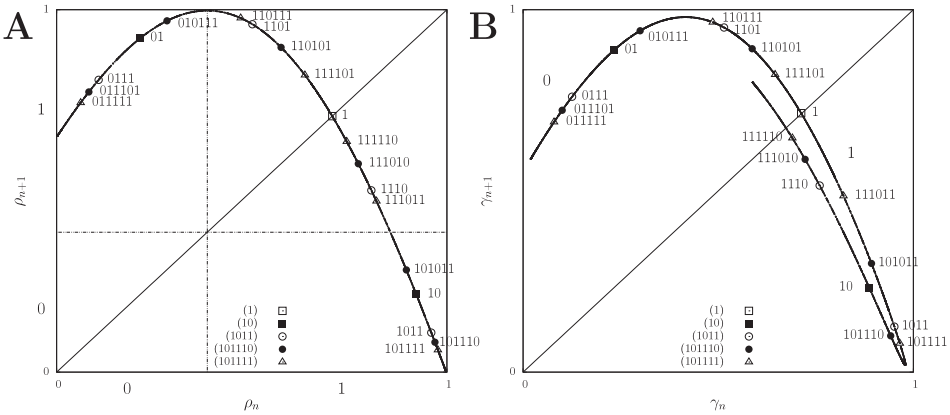

Fig. 7. Comparison of periodic points order in first return maps. First return maps of two equivalents Poincaré sections for the Rössler system with periodic points of the unstable periodic orbits. A and B correspond respectively to Poincaré section (2) and (6). As these two first return maps are obtained from equivalent Poincaré sections, the relative order of the periodic points is conserved by following the line in A and B. This translates the fact that the stretching and folding mechanism start in the three-dimensional space inducing modification in the structure of the first return map B compared to A. In addition, the relative order of periodic points corresponds to ρ_n values in A while it does not correspond to the order of γ_n values in B.

that is represented in Fig. 6. From this first return map, a variable γ_n is build to represent the distance from the inside to the outside of the attractor as it has been done for ρ_n (2):

$$\gamma_n = (y_n - 0.229)/(1.7634 - 0.229). \tag{7}$$

As illustrated by Fig. 6B, such a construction implies the loss of bijection from the Poincaré section $\mathcal{Q}$ to γ_n. Facing this extra branch in first return map, one can be tempted to consider that there are three branches in the template with an encoding that could be 0, 1 and $\bar{1}$. Instead of trying to study directly the extra-branch impact from the first return map Fig. 7B, we proposed to build a bijective representation of $\mathcal{Q}$ using η_n that is defined as follows:

$$\eta_n = \begin{cases} (y_n - 0.229)/(1.7634 - 0.229) & \text{if } z_n \leq -1.1665 \\ 1 + (y_n - 1.137)/(1.7634 - 1.137) & \text{else} \end{cases} \tag{8}$$

Such a partition of the Poincaré section implies a separation and this is used to characterise chaotic attractor bounded by higher genus torus where multiple components are required to study their topology [59,60]. The first return map associated to this representation of the Poincaré section $\mathcal{Q}$ with η_n is represented Fig. 8A.

Consequently, η_n has values between 0 and 1 giving the increasing and decreasing branches encoded with 0 and 1 from γ_n and values of η_n between 1 and 2 corresponds to the values of the additional decreasing branch from γ_n and is encoded with $\bar{1}$. The first return map (Fig. 8A) associated to such a Poincaré section clearly split the three branches and indicates that there are only three transitions between the components:

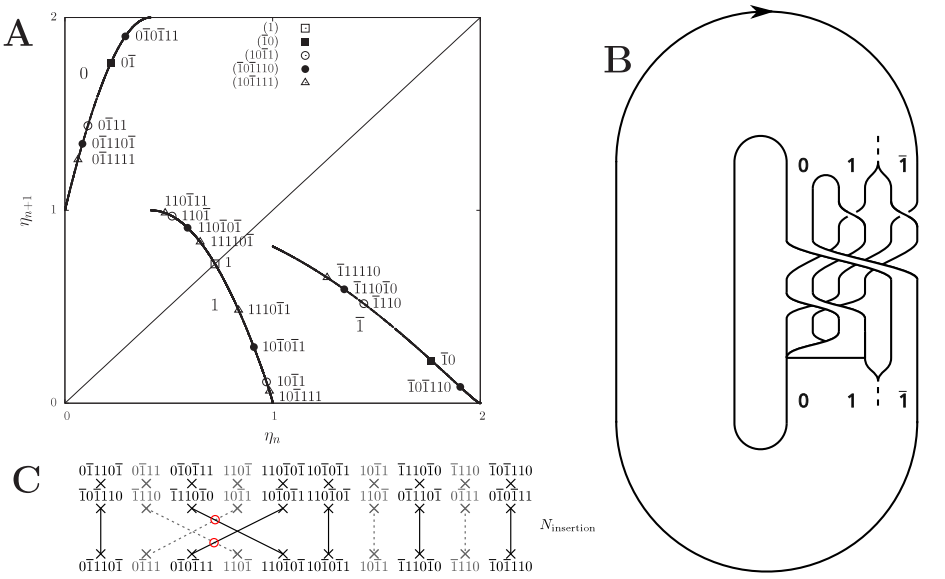

Fig. 8. Topological characterisation of the Rössler attractor considering three distinct branches. A. First return map of a Poincaré section with two components, separating out the additional decreasing branch. From branch 0, only transition to branch $\bar{1}$ are possible. B. Template with three branches including a separation between the two components. The separation between 1 and $\bar{1}$ is virtual as it is underlined by dashed line. (9) is the linking matrix describing this template. C. Linking graph used to theoretically compute linking numbers between orbits $N_{\text{insertion}} = 2$ (10).

- From branch 0, the next periodic point will be in branch $\bar{1}$.
- From branch $\bar{1}$, the next periodic point will be in branches 0 or 1.
- From branch 1, the next periodic point will be in branches 0 or 1.

The hypothesis of separating the two decreasing branches leads us to a template (Fig. 8B) described by the linking matrix R_3:

$$R_3 = \begin{matrix} 0 \\ 1 \\ \bar{1} \end{matrix} \begin{bmatrix} 0 & -1 & -1 \\ -1 & -1 & -1 \\ -1 & -1 & -1 \end{bmatrix} . \tag{9}$$

with the following structure (Fig. 8B). This template is also validated using numerical and theoretical linking numbers. This calculation for two periodic orbits of period 4 and 6 is:

$$\begin{aligned} lk(10\bar{1}1, 10\bar{1}0\bar{1}1) &= \frac{1}{2}\left[2R_{0,0} + 6R_{0,1} + 4R_{0,\bar{1}} + 4R_{1,1} + 6R_{1,\bar{1}} + 2R_{\bar{1},\bar{1}} + N_{\text{insertion}}\right] \\ &= \frac{1}{2}(0 - 6 - 4 - 4 - 6 - 2 + 2) = -10 , \end{aligned} \tag{10}$$

including the insertion number computed theoretically (Fig. 8C).

Considering that both torsions of branch 1 and $\bar{1}$ are equal to -1 and that they permute negatively once, they can be regrouped in a unique negative torsion. Consequently, the template with three branches (Fig. 8B) is topologically equivalent to the Rössler template with two branches (Fig. 1G). Therefore, splitting the first return map into three branches produces the same result as considering only two branches and reordering the periodic points based on their implication number that corresponds to the progression from one side to the other on the first return map. As the Poincaré section leading to this calculation are equivalents, (2) and (6), the additional branch appears because of the positioning of Poincaré section (6) in the chaotic mechanism where stretching and folding are occurring and before the squeezing mechanism. Consequently, even if the Poincaré section is not ideally positioned to analyse the topology of a chaotic attractor, the shape of its first return map synthesises the chaotic mechanism without the need of considering additional branches as being new interesting branches from the topological perspective.

5. Template and its implication

5.1. Template of the model

Further to the results of previous section, the topological method is applied directly without considering the layers of $\mathcal{E}$. Thus, ρ_n is a discrete value detailing successive passage of the flow through the Poincaré section, allowing the drawing of a first-return

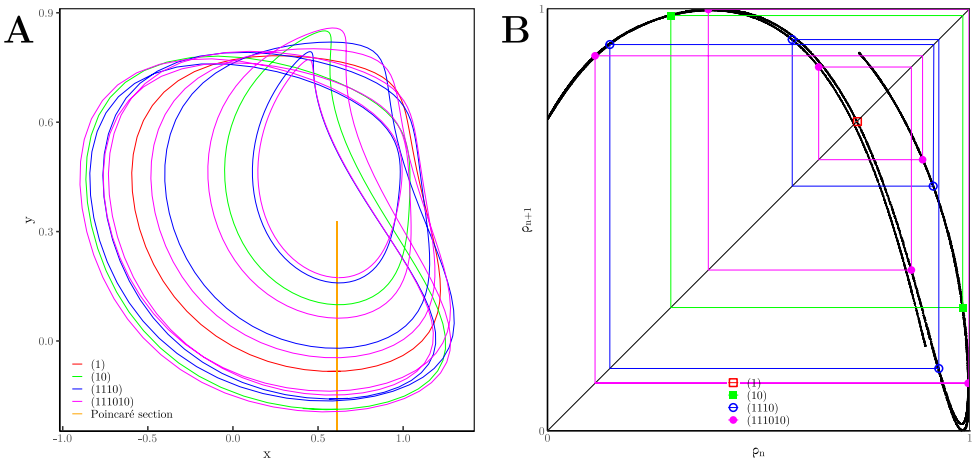

Fig. 9. (**A**) A set of 4 orbits of the attractor $\mathcal{E}$. (**B**) The first return map associated to $\mathcal{P}$. The 4 orbits are plotted on it. The coordinates are normalised between 0 and 1 (11).

Table 2
Numerical linking numbers between pairs of orbits extracted from the chaotic attractor $\mathcal{E}$.

	(1)	(10)	(1110)
(10)	−1		
(1110)	−2	−3	
(111010)	−3	−5	−10

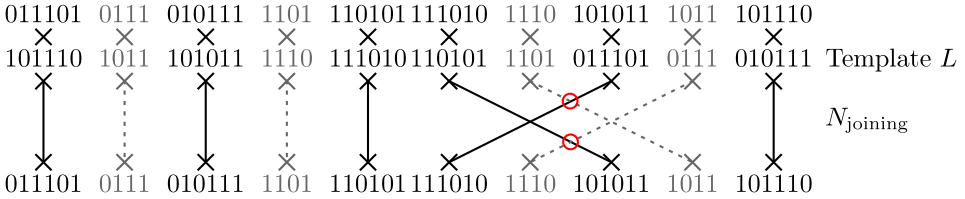

Fig. 10. Theoretical computation of N_{joining} for $lk(1110, 111010)$. Each positive crossing is counted: $N_{\text{joining}} = 2$.

map that describes the dynamic of the flow in one dimension.

$$\rho_n = \frac{-y - \min(y)}{\max(y) - \min(y)} \tag{11}$$

The unstable periodic orbits (Fig. 9.A) are extracted from the attractor $\mathcal{E}$. The first-return map (Fig. 9.B) is subsequently plotted along with the orbits. Based on the work previously detailed (Section 4.2), only two branches are considered which leads to the naming convention, 0 and 1, used in Fig. 9, Tables 2 and 3. The symbol 0 is for the increasing branch and the symbol 1 for the decreasing branch. The linking numbers are computed using a script written in Python [61], giving numbers identical to the one obtained by an analysis of the Rössler system (Fig. 1). The same template and its associated linking matrix are considered:

$$L = \begin{bmatrix} 0 & -1 \\ -1 & -1 \end{bmatrix}.$$

The computation of the theoretical linking numbers is then done (and detailed in 3) using the following formula:

$$lk(\mathcal{O}, \mathcal{O}') = \frac{1}{2} \times \left(\sum_{i=1}^{k} \sum_{j=1}^{l} L_{\mathcal{O}_i, \mathcal{O}'_j} + N_{\text{joining}}(\mathcal{O}, \mathcal{O}') \right)$$

As the theoretical linking numbers correspond to numerical ones, template is validated (Fig. 1e). This template evolving clockwise is made of a continuous part from bottom right to top right. The remaining part is composed of the chaotic mechanism made with two branches: 0 that has no torsion and 1 with a negative torsion permuting with the other branch, stretching and reversing the order of orbits in the flow until both branches are squeezed together.

Table 3
Theoretical linking numbers between pairs of orbits extracted from the chaotic attractor $\mathcal{E}$ (see Fig. 10 for examples of N_{joining} computation).

$lk(1,1110) = \frac{1}{2} \times [3L_{1,1} + L_{1,0} + N_{\text{joining}}]$ $= \frac{1}{2} \times (-3 - 1 + 0) = -2$
$lk(10,1110) = \frac{1}{2} \times [3L_{1,1} + L_{1,0} + 3L_{0,1} + L_{0,0} + N_{\text{joining}}]$ $= \frac{1}{2} \times (-3 - 1 - 3 + 0 + 1) = -3$
$lk(1110,111010) = \frac{1}{2} \times [3 \times 4L_{1,1} + 3 \times 2L_{1,0} + 4L_{0,1} + 2L_{0,0} + N_{\text{joining}}]$ $= \frac{1}{2} \times (-12 - 6 - 4 + 0 + 2) = -10$

5.2. Interpretation and discussion

The main interest of the template representation is that it reproduces all properties of chaotic solutions. First, the solution is bounded in the template. Secondly, the evolution is not time-dependent because it is built on topological invariants. Finally, the last part of the chaotic mechanism with stretching and squeezing illustrates the sensitivity to initial conditions as well as the nondeterministic properties by allowing all trajectories to be redistributed in every branch for the next topological period. The topological structure of the attractor $\mathcal{E}$ indicates where the mechanisms leading to chaos occur: stretching to split closed trajectories and folding and squeezing to mix them while maintaining a bounded evolution of the trajectories. This mechanism is detailed theoretically Fig. 1e where the periodic orbits are embedded in the template of $\mathcal{R}$ that is equal to the template of $\mathcal{E}$. Two branches are distinguished where the left part contains no torsion, and the external branch has a negative torsion. Orbits of the attractor $\mathcal{E}$ (Fig. 9A) are spatially closed to the theoretical representation of the template except that there is an additional branch. The latter indicates that for a couple (x, y) (unemployment and inflation) two distinct values of z (exchange rate) (Fig. 5B) have non equivalent values at the end of the chaotic mechanism in the template. The stretching, folding and squeezing occur in the chaotic mechanism of the template while a part of the attractor will be squeezed later in the chaotic mechanism after a revolution. The trajectories on the right of the Poincaré section of Fig. 9A reproduces transformations due to the chaotic mechanism of the attractor. As mentioned before, for $\mathcal{E}$, there is no place to position the Poincaré section without having this additional branch. This branch is visible all along the flow with two layers.

From an economic point of view, when unemployment decrease, price inflation tends to accelerate with possibly two distinct values of exchange rates due to this additional branch. This parallel evolution of trajectories (which corresponds to the theoretical form of the Phillips curve) is maintained until stretching and folding occur to mix trajectories, that is, when both x and y, respectively, unemployment and inflation are high (Fig. 9A). This phenomenon precedes the torsion and squeezing part of the template in the phase space. In this area, there are several possibilities for closed trajectories, it includes both scenarios where two closed trajectories will diverge to follow distinct paths or, two distinct trajectories could also be closed after the chaotic mechanism because of the squeezing mechanism. Another possibility is that two distinct trajectories could exchange their relative positions because at the end of the template, the branches are stretched and squeezed to the branch line.

The coexistence of high inflation and high unemployment directly contradicts the conventional Phillips curve framework. This phenomenon known as "stagflation", which was particularly observed during the 1970s, has necessitated a re-evaluation of the factors driving inflation and unemployment, prompting economists to consider alternative explanations (supply-side shocks, role of inflationary expectations). Beyond these dimensions that are not addressed in the paper, our empirical approach suggests that the juxtaposition of high unemployment and high inflation can lead to a chaotic dynamic, that is, an unpredictable dynamical regime despite the underlying determinism.

6. Conclusion

From economic data time series, a model has been generated using a global modelling tool. A model defined by a three-differential equations system has been obtained, that will hopefully pave the way and bring up interest to the study of non-linear, chaotic dynamics and global modelling based on economic data. The system cannot be classified as an economic model ; however, being derived from data, it encapsulates underlying relationships between unemployment, inflation and nominal exchange rate. The solution of the model is a chaotic attractor that has been subsequently topologically characterised. We proved that the presence of a supplementary branch does not raise any issue in the topological analysis of the attractor $\mathcal{E}$, which is topologically equivalent to that of the classical Rössler attractor. In terms of economic analysis, our study complements existing empirical approaches by applying a topological analysis to "classical" economic data, which provides insights into the complex and nonlinear interactions among multiple economic variables. This exploratory approach suggests the exchange rate plays a role in the inflation-unemployment relationship: it could lead to very different dynamics that may be considered in theoretical modelling. More important, the analysis

allowed the identification of key point in chaotic dynamics specifically during periods of high inflation and high unemployment – and not elsewhere – thereby indicating where trajectories intertwine and concentrate. The simultaneous occurrence of inflation and unemployment presents a conundrum that challenges traditional macroeconomic models, particularly those based on the Phillips curve, which posits an inverse relationship between these two economic aggregates. In this context, it could be viewed as a potential shift to another economic regime, driven by factors that introduce non-linearities and sensitivity to initial conditions, characteristics of chaotic systems. For future works, we plan to realise bifurcation diagrams of the differential equation system to fully understand the route to chaos by varying parameters and contribute to a better understanding of the rise of chaotic dynamics in the model and its potential role in the economical phase space.

CRediT authorship contribution statement

Alexandre Meneceur: Writing – review & editing, Writing – original draft, Visualization, Software, Resources, Investigation, Formal analysis, Data curation. **Vincent Lignon:** Writing – review & editing, Writing – original draft, Visualization, Supervision, Project administration, Funding acquisition, Conceptualization. **Martin Rosalie:** Writing – review & editing, Writing – original draft, Visualization, Supervision, Project administration, Methodology, Funding acquisition, Conceptualization.

Declaration of competing interest

The authors declare that they have no known competing financial interests or personal relationships that could have appeared to influence the work reported in this paper.

Acknowledgements

This work has benefited from the support of the 'Fédération de Recherche Energie et Environnement' (FREE 2043 CNRS-UPVD) awarded to both Vincent Lignon and Martin Rosalie. This study is set within the framework of the "Laboratoires d'Excellences (LABEX)" TULIP (ANR-10-LABX-41) and of the "École Universitaire de Recherche (EUR)" TULIP-GS (ANR-18-EURE-0019). The authors thanks Sylvain Mangiarotti for helpful comments and remarks. The authors would like to thank the editor and the anonymous reviewers for their valuable comments and suggestions, which helped improve the quality of this paper.

Data availability

The code and data supporting the findings of this study are openly available on GitHub at https://github.com/ameneceur/economic-attractor-topology.

References

[1] Barnett WA, Serletis A, Serletis D. Nonlinear and complex dynamics in economics. Macroecon Dyn 2014;19(8):1749–79. http://dx.doi.org/10.1017/s1365100514000091.
[2] Baumol W, Benhabib J. Chaos: Significance, mechanism, and economic applications. J Econ Perspect 1989;3(1):77–105, URL http://www.jstor.org/stable/1942966.
[3] Day RH. The emergence of chaos from classical economic growth. Q J Econ 1983;98(2):201–13. http://dx.doi.org/10.2307/1885621.
[4] Olmedo E. Is there chaos in the Spanish labour market? Chaos Solitons Fractals 2011;44(12):1045–53. http://dx.doi.org/10.1016/j.chaos.2011.08.001.
[5] Faggini M. Chaotic time series analysis in economics: Balance and perspectives. Chaos: An Interdiscip J Nonlinear Sci 2014;24(4). http://dx.doi.org/10.1063/1.4903797.
[6] Glass L. Introduction to controversial topics in nonlinear science: Is the normal heart rate chaotic? Chaos: An Interdiscip J Nonlinear Sci 2009;19(2):028501. http://dx.doi.org/10.1063/1.3156832.
[7] Bischi GI. From Samuelson's multiplier-accelerator to bifurcations and chaos in economic dynamics. Decis Econ Finance 2024. http://dx.doi.org/10.1007/s10203-024-00462-0.
[8] Faggini M, Parziale A. More than 20 years of chaos in economics. Mind & Soc 2015;15(1):53–69. http://dx.doi.org/10.1007/s11299-015-0164-1.
[9] Faggini M. Chaos detection in economic time series: Metric versus topological tools. In: Ltd S, editor. Adv Manag Appl Econ 2013;3(6):27–52, URL https://www.scienpress.com/journal_focus.asp?main_id=55&Sub_id=IV&Issue=932.
[10] Phillips AW. The relation between unemployment and the rate of change of money wage rates in the United Kingdom, 1861-1957. Economica 1958;25(100):283–99. http://dx.doi.org/10.2307/2550759, arXiv:2550759.
[11] Lavoie M. Conflictual inflation and the Phillips curve. Rev Political Econ 2024;36(4):1397–419. http://dx.doi.org/10.1080/09538259.2023.2294305.
[12] Gordon RJ. The history of the Phillips curve: Consensus and bifurcation. Economica 2011;78(309):10–50, URL https://www.jstor.org/stable/41236106.
[13] Geerolf F. The Phillips Curve: A relation between real exchange rate growth and unemployment. 2020, URL https://fgeerolf.com/phillips.pdf.
[14] Mangiarotti S, Coudret R, Drapeau L, Jarlan L. Polynomial search and global modeling: Two algorithms for modeling chaos. Phys Rev E 2012;86:046205. http://dx.doi.org/10.1103/PhysRevE.86.046205.
[15] Boulant G, Lefranc M, Bielawski S, Derozier D. Horseshoe templates with global torsion in a driven laser. Phys Rev E 1997;55(5):5082–91. http://dx.doi.org/10.1103/physreve.55.5082.
[16] Barrio R, Lefranc M, Martínez MA, Serrano S. Symbolic dynamical unfolding of spike-adding bifurcations in chaotic neuron models. Europhys Lett 2015;109(2):20002. http://dx.doi.org/10.1209/0295-5075/109/20002.
[17] Letellier C, Olsen LF, Mangiarotti S. Chaos: From theory to applications for the 80th birthday of Otto E. Rössler. Chaos: An Interdiscip J Nonlinear Sci 2021;31(6):060402. http://dx.doi.org/10.1063/5.0058332.
[18] Boulant G, Lefranc M, Bielawski S, Derozier D. A nonhorseshoe template in a chaotic laser model. Int J Bifurc Chaos 1998;08(05):965–75. http://dx.doi.org/10.1142/s0218127498000772.

[19] Aguirre LA, Letellier C, Maquet J. Forecasting the time series of sunspot numbers. Sol Phys 2008;249(1):103–20. http://dx.doi.org/10.1007/s11207-008-9160-5.
[20] Abadie M, Beck P, Parker JP, Schneider TM. The topology of a chaotic attractor in the Kuramoto–Sivashinsky equation. Chaos: An Interdiscip J Nonlinear Sci 2025;35(1). http://dx.doi.org/10.1063/5.0237476.
[21] Letellier C, Ménard O, Klinger T, Piel A, Bonhomme G. Dynamical analysis and map modeling of a thermionic diode plasma experiment. Phys D: Nonlinear Phenom 2001;156(1–2):169–78. http://dx.doi.org/10.1016/s0167-2789(01)00279-2.
[22] Kamdoum Tamba V, Fotsin HB, Kengne J, Megam Ngouonkadi EB, Talla PK. Emergence of complex dynamical behaviors in improved Colpitts oscillators: antimonotonicity, coexisting attractors, and metastable chaos. Int J Dyn Control 2016;5(3):395–406. http://dx.doi.org/10.1007/s40435-016-0223-4.
[23] Rössler OE. An equation for continuous chaos. Phys Lett A 1976;57(5):397–8. http://dx.doi.org/10.1016/0375-9601(76)90101-8.
[24] Aguirre LA, Letellier C. Modeling nonlinear dynamics and chaos: A review. Math Probl Eng 2009;2009:1–35. http://dx.doi.org/10.1155/2009/238960.
[25] Gilmore R, Lefranc M. The topology of chaos: Alice in stretch and squeezeland. Wiley; 2012, http://dx.doi.org/10.1002/9783527639403.
[26] Letellier C, Dutertre P, Maheu B. Unstable periodic orbits and templates of the Rössler system: Toward a systematic topological characterization. Chaos: An Interdiscip J Nonlinear Sci 1995;5(1):271–82. http://dx.doi.org/10.1063/1.166076.
[27] Rosalie M, Mangiarotti S. Structure analysis of the Lorenz-84 chaotic attractor. Chaos: An Interdiscip J Nonlinear Sci 2025;35(10). http://dx.doi.org/10.1063/5.0287725.
[28] Gilmore R. Topological analysis of chaotic dynamical systems. Rev Modern Phys 1998;70(4):1455. http://dx.doi.org/10.1103/RevModPhys.70.1455.
[29] Birman JS, Williams R. Knotted periodic orbits in dynamical systems—I: Lorenz's equation. Topology 1983;22(1):47–82. http://dx.doi.org/10.1016/0040-9383(83)90045-9.
[30] Tufillaro NB, Solari HG, Gilmore R. Relative rotation rates: Fingerprints for strange attractors. Phys Rev A 1990;41(10):5717–20. http://dx.doi.org/10.1103/physreva.41.5717.
[31] Rosalie M. Templates and subtemplates of Rössler attractors from a bifurcation diagram. J Phys A 2016;49(31):315101. http://dx.doi.org/10.1088/1751-811/3/49/31/315101.
[32] Crutchfield JP, McNamara BS. Equations of motion from a data series. Complex Systems 1987;1:417–52, URL https://www.complex-systems.com/abstracts/v01_i03_a03/.
[33] Aguirre LA, Billings SA. Improved structure selection for nonlinear models based on term clustering. Internat J Control 1995;62(3):569–87. http://dx.doi.org/10.1080/00207179508921557.
[34] Gouesbet G, Letellier C. Global vector-field reconstruction by using a multivariate polynomial L_2 approximation on nets. Phys Rev E 1994;49(6):4955–72. http://dx.doi.org/10.1103/physreve.49.4955.
[35] Gouesbet G. Reconstruction of the vector fields of continuous dynamical systems from numerical scalar time series. Phys Rev A 1991;43(10):5321–31. http://dx.doi.org/10.1103/physreva.43.5321.
[36] Letellier C, Le Sceller L, Maréchal E, Dutertre P, Maheu B, Gouesbet G. Global vector field reconstruction from a chaotic experimental signal in copper electrodissolution. Phys Rev E 1995;51(5):4262–6. http://dx.doi.org/10.1103/physreve.51.4262.
[37] Mangiarotti S. Low dimensional chaotic models for the plague epidemic in Bombay (1896–1911). Chaos Solitons Fractals 2015;81:184–96. http://dx.doi.org/10.1016/j.chaos.2015.09.014.
[38] Mangiarotti S, Huc M. Can the original equations of a dynamical system be retrieved from observational time series? Chaos: An Interdiscip J Nonlinear Sci 2019;29(2):023133. http://dx.doi.org/10.1063/1.5081448.
[39] Brunton SL, Proctor JL, Kutz JN. Discovering governing equations from data by sparse identification of nonlinear dynamical systems. Proc Natl Acad Sci USA 2016;113(15):3932–7. http://dx.doi.org/10.1073/pnas.1517384113.
[40] Mangiarotti S, Drapeau L, Letellier C. Two chaotic global models for cereal crops cycles observed from satellite in northern Morocco. Chaos: An Interdiscip J Nonlinear Sci 2014;24(2). http://dx.doi.org/10.1063/1.4882376.
[41] Mangiarotti S, Zhang Y, Leblanc M. Chaos theory applied to the modelling of karst springs: first results from univariate time series. Hydrogeol J 2019;27(6):2027–43. http://dx.doi.org/10.1007/s10040-019-01971-8.
[42] Mangiarotti S, Peyre M, Zhang Y, Huc M, Roger F, Kerr Y. Chaos theory applied to the outbreak of COVID-19: an ancillary approach to decision making in pandemic context. Epidemiology & Infect 2020;148:e95. http://dx.doi.org/10.1017/S0950268820000990.
[43] Mangiarotti S, Fu E, Jouquet P, Tran M, Huc M, Bottinelli N. Earthworm activity and its coupling to soil hydrology: A deterministic analysis. Chaos: An Interdiscip J Nonlinear Sci 2021;31(1). http://dx.doi.org/10.1017/S0950268820000990.
[44] Sáez M, Benavente D, Cuezva S, Huc M, Fernández-Cortés Á, Mialon A, et al. Scenarios for the Altamira cave CO_2 concentration from 1950 to 2100. Sci Rep 2024;14(1):10359. http://dx.doi.org/10.1038/s41598-024-60149-9.
[45] Mangiarotti S, Le Jean F, Chassan M, Drapeau L, Huc M. GPoM: Generalized Polynomial Modelling, package on CRAN. 2012, URL https://cran.r-project.org/package=GPoM.
[46] Leclerc H, INSEE. Insee: Tools to easily download data from INSEE BDM database. 2024, URL https://cran.r-project.org/web/packages/insee/index.html.
[47] Schumann E. BISdata: Download data from the Bank for International Settlements (BIS). 2024, URL https://cran.r-project.org/web/packages/BISdata/index.html.
[48] Kwiatkowski D, Phillips PC, Schmidt P, Shin Y. Testing the null hypothesis of stationarity against the alternative of a unit root. J Econometrics 1992;54(1–3):159–78. http://dx.doi.org/10.1016/0304-4076(92)90104-y.
[49] Phillips PCB, Perron P. Testing for a unit root in time series regression. Biometrika 1988;75(2):335–46. http://dx.doi.org/10.1093/biomet/75.2.335.
[50] Dickey DA, Fuller WA. Distribution of the estimators for autoregressive time series with a unit root. J Amer Statist Assoc 1979;74(366a):427–31. http://dx.doi.org/10.1080/01621459.1979.10482531.
[51] Trapletti A, Hornik K. tseries: Time series analysis and computational finance. 1999, http://dx.doi.org/10.32614/cran.package.tseries.
[52] Letellier C, Aguirre LA, Freitas US. Frequently asked questions about global modeling. Chaos: An Interdiscip J Nonlinear Sci 2009;19(2). http://dx.doi.org/10.1063/1.3125705.
[53] Soliman AS. Transitions from stable equilibrium points to periodic cycles to chaos in a Phillips curve system. J Macroecon 1996;18(1):139–53. http://dx.doi.org/10.1016/S0164-0704(96)80008-5.
[54] Aguirre LA, Letellier C. Nonstationarity signatures in the dynamics of global nonlinear models. Chaos: An Interdiscip J Nonlinear Sci 2012;22(3). http://dx.doi.org/10.1063/1.4748852.
[55] Lorenz EN. Deterministic nonperiodic flow. J Atmos Sci 1963;20(2):130–41. http://dx.doi.org/10.1175/1520-0469(1963)020<0130:dnf>2.0.co;2.
[56] Chen G, Ueta T. Yet another chaotic attractor. Int J Bifurc Chaos 1999;9(07):1465–6. http://dx.doi.org/10.1142/S0218127499001024.
[57] Rosalie M. Templates of two foliated attractors — Lorenz and Chen systems. Int J Bifurc Chaos 2016;26(02):1650037. http://dx.doi.org/10.1142/s0218127416500371.
[58] Rosalie M, Letellier C. Systematic template extraction from chaotic attractors: II. Genus-one attractors with multiple unimodal folding mechanisms. J Phys A 2015;48(23):235101. http://dx.doi.org/10.1088/1751-8113/48/23/235101.
[59] Tsankov TD, Gilmore R. Topological aspects of the structure of chaotic attractors in R^3. Phys Rev E - Stat Nonlinear, Soft Matter Phys 2004;69(5):056206. http://dx.doi.org/10.1103/PhysRevE.69.056206.
[60] Rosalie M, Letellier C. Toward a general procedure for extracting templates from chaotic attractors bounded by high genus torus. Int J Bifurc Chaos 2014;24(04):1450045. http://dx.doi.org/10.1142/s021812741450045x.
[61] Uribarri G, Mindlin GB. The structure of reconstructed flows in latent spaces. Chaos: An Interdiscip J Nonlinear Sci 2020;30(9):093109. http://dx.doi.org/10.1063/5.0013714.